Science of the Total Environment 624 (2018) 133–144

Contents lists available at ScienceDirect

Science of the Total Environment

journal homepage: www.elsevier.com/locate/scitotenv

Sequential samples reveal significant variation of mercury isotope ratios during single rainfall events

Shengliu Yuan [a,b], Jiubin Chen [a,*], Hongming Cai [a], Wei Yuan [a,b], Zhongwei Wang [a,b], Qiang Huang [a], Yujie Liu [a], Xingyang Wu [c]

[a] State Key laboratory of Environmental Geochemistry, Institute of Geochemistry, Chinese Academy of Sciences, 99 Linchengxi Road, Guiyang, Guizhou 550081, China
[b] University of Chinese Academy of Sciences, Beijing 100049, China
[c] Meteorological Information Center of Guizhou, Guiyang 550002, China

HIGHLIGHTS

- Hg isotope ratios were measured in sequential precipitation for 3 events.
- Contribution of different sources was observed due to meteorological conditions.
- Particulate Hg and filtered rainwater Hg showed different isotopic compositions.
- Isotopic composition was sensitive to a brief anthropogenic incense burning event.

GRAPHICAL ABSTRACT

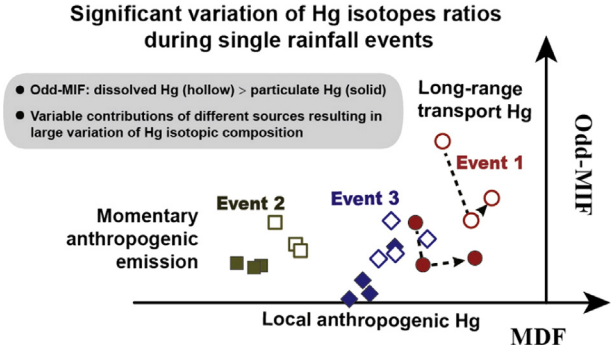

ARTICLE INFO

Article history:
Received 6 August 2017
Received in revised form 4 December 2017
Accepted 7 December 2017
Available online 14 December 2017

Editor: Mae Mae Sexauer Gustin

Keywords:
Mercury isotopes
Wet deposition dynamic
Particulate phase
Filtered phase
Hydrogen and oxygen isotopes
Incense burning

ABSTRACT

Although the investigation of mercury (Hg) isotopes in precipitation has largely improved our knowledge of the source and transformation of Hg in the atmosphere, rainwater investigated in previous studies were integrated samples collected over an event and could obscure key information about the physiochemical transformation and deposition dynamics of Hg (and its isotopes) in short precipitation events. In this study, we investigated Hg isotopic composition of filtered (Hg_F) and particulate Hg (Hg_{PM}) in sequential rain samples from three single rainfall events in Guiyang, China. All samples showed a decrease of total Hg concentration, as well as Hg_F and Hg_{PM} with time in each rainfall event, and large variation of both mass-dependent fractionation (MDF) and mass-independent fractionation of odd Hg isotopes (odd-MIF) for both phases. Isotopic data indicated variable contributions of different sources triggered by the instant change of meteorological conditions, rather than internal atmospheric processes. The rapid response of MDF and odd-MIF of precipitation samples to the incense burning on the Tomb Sweeping Day implied that Hg isotopic composition was very sensitive to the momentary anthropogenic emission, which could have at least a regional short-lived effect and should be taken into account in future studies. Hg isotopes are a powerful tool for investigating both atmospheric transformation and instant deposition dynamic of Hg, and like stable H and O isotopes, could provide useful information about local or regional meteorological changes.

* Corresponding author.
E-mail address: chenjiubin@vip.gyig.ac.cn (J. Chen).

https://doi.org/10.1016/j.scitotenv.2017.12.082
0048-9697/

1. Introduction

Mercury (Hg) is a globally transported contaminant (Giang and Selin, 2015). The atmosphere is both a receptor of naturally and anthropogenically emitted Hg, and a crucial contributing source of Hg in surface ecosystem through both wet (mainly in reactive gaseous Hg (RGM) and particulate Hg (PHg)) and dry deposition (mainly in PHg and gaseous elemental Hg, GEM) (Enrico et al., 2016, 2017; Landing et al., 2010; Lynam et al., 2014; Marumoto and Matsuyama, 2014; Obrist et al., 2017; Sanei et al., 2010; Schroeder and Munthe, 1998). Previous studies have shown that the majority of atmospheric Hg is transported to the surface through wet deposition, because RGM and PHg are both prone to scavenging (Lynam et al., 2014; Seo et al., 2012). Inorganic Hg derived from the atmosphere is converted into methylmercury (MeHg) that impacts the health of humans and biota (Giang and Selin, 2015; Walters et al., 2015). Thus, understanding Hg deposition dynamics is important for deciphering the biogeochemical cycling of Hg in surface terrestrial ecosystems. Although significant progress has been made on the understanding of atmospheric Hg deposition through investigation of Hg concentration, species and transport models, some aspects of the deposition flux and dynamics remain unclear (Brunke et al., 2016; Gratz et al., 2009; Huang et al., 2012; Seo et al., 2012; White et al., 2013).

Measurement of Hg isotopes has proven useful for investigating the transformation and the flux of Hg between different reservoirs (Blum et al., 2014). Recent studies have reported both mass-dependent fractionation of Hg isotopes (MDF, δ^{202}Hg) and mass-independent fractionation of odd Hg isotopes (odd-MIF, Δ^{199}Hg and Δ^{201}Hg) in both natural samples (sediments, soils, food web and precipitation) (Blum et al., 2014; Sun et al., 2014, 2016) and in laboratory experiments (Bergquist and Blum, 2007; Zheng and Hintelmann, 2009, 2010). Odd-MIF is mainly induced by specific biogeochemical processes, such as divalent Hg photo-reduction, abiotic dark reduction, MeHg photo-degradation, and elemental Hg evaporation, and is triggered by either the magnetic isotope effect (MIE) or the nuclear volume effect (NVE) (Bergquist and Blum, 2007; Blum et al., 2014; Sun et al., 2016; Zheng and Hintelmann, 2009, 2010). Though the exact mechanisms remain unclear, MIF of even Hg isotopes (even-MIF, Δ^{200}Hg) has also been recently determined in atmospheric samples or natural materials mainly related to the atmosphere, such as GEM (Demers et al., 2015; Rolison et al., 2013), precipitation Hg (including both RGM and PHg) (Chen et al., 2012; Gratz et al., 2010; Sherman et al., 2012; Z. Wang et al., 2015; Yuan et al., 2015), mosses (Cai and Chen, 2016), sediments and soils (Demers et al., 2013; Gray et al., 2013, 2015). This renders Hg a unique heavy metal having a "three-dimensional" isotope system (Cai and Chen, 2016; Chen et al., 2012).

Hg isotopes have been successfully used to trace atmospheric Hg sources and transport. The studies on the integrated precipitation samples (mixing the samples of successive precipitation events over days or even weeks) from USA showed that Hg isotopic compositions could serve as an efficient tracer of local and regional emission (Gratz et al., 2010; Sherman et al., 2012, 2015). Two studies of precipitation in China and Canada demonstrated that Hg isotopes could be used for tracking long-range transport as well (Chen et al., 2012; Z. Wang et al., 2015). Moreover, Hg isotopes could be employed in much more complex systems for assessing sources or behaviors of its subspecies (Demers et al., 2013, 2015). Interestingly, even isotope anomaly has been observed in all atmospheric samples and could be used as a conservative tracer of upper atmosphere chemistry (Cai and Chen, 2016; Chen et al., 2012, 2016; Demers et al., 2013, 2015; Gratz et al., 2010; Sherman et al., 2012, 2015; Z. Wang et al., 2015; Yuan et al., 2015). These studies demonstrated that both odd-MIF and even-MIF could serve as the Hg deposition tracer from atmosphere to earth surface.

Due to the need of enough mass of Hg for high-precision isotope measurement, the precipitation samples investigated in the above studies are all integrated samples collected from an entire precipitation event or from multiple events, over a relatively long period. This sampling scheme obscures some key information about the physiochemical transformation of Hg (and its isotopes) related to the washout curve. For example, studies with high frequency sequential sampling has reported the great variability of Hg concentration in intra-rainfall events (White et al., 2009, 2013), which might be caused by the changes of meteorological conditions, source contribution and/or other potential factors (White et al., 2013). These changes would also induce large variation of isotope ratios, as demonstrated in previous studies for other stable isotopes (e.g. δ^2H-H_2O, δ^{18}O-H_2O, and δ^{15}N-NO_3^-) (Coplen et al., 2008; Felix et al., 2015; Li et al., 2015; Munksgaard et al., 2012). Similarly, in our previous study, variation of both MDF and MIF of Hg isotopes were also observed in one single rain event at the Lhasa City on the Tibetan Plateau (Yuan et al., 2015) that likely resulted from the contribution of variable Hg sources characterized by different isotopic compositions (Chen et al., 2012; Gratz et al., 2010; Sherman et al., 2012; Z. Wang et al., 2015; Yuan et al., 2015). This observation motivated further systematic study of changes in Hg isotopes during intra-precipitation events and the relative influence of contributory factors in other geographic regions.

Here, we conducted a systematic study of Hg concentration and isotopic variations in sequential samples collected from three intra-rainfall events at Guiyang City, China. The potential factors causing these variations were carefully investigated by coupling Hg, oxygen and hydrogen isotopic signatures, meteorological data, and air-mass back trajectory calculation. Because the particulate phase could occupy a large proportion of total Hg (Huang et al., 2012, 2013), we collected and measured Hg concentrations and isotopic ratios in filtered rainfall (Hg_F) and on particles (Hg_{PM}) separately. Many previous studies investigated bulk unfiltered rainfall only. The specific objectives are 1) to investigate the variation of Hg concentration and isotopic composition in the particulate and filtered phases during single rainfall events; 2) to identify the potential factors controlling these variations; and, 3) to test the possibility of tracing meteorological changes using Hg isotopes.

2. Materials and methods

2.1. Materials and reagents

All reagents, including HCl, HNO_3, KBr, $KBrO_3$, L-cysteine, $NH_2OH{\cdot}HCl$ and $SnCl_2$, were analytical grade (Sinopharm Chemical Reagent Co., Ltd., China) and were prepared in an ultra-clean room at the Institute of Geochemistry, Chinese Academy of Sciences (IGCAS). 18.2 MΩ Milli-Q water (Millipore, USA) was used for preparation all aqueous solutions. Concentrated HCl and HNO_3 were double-distilled. A 0.2 M BrCl solution was prepared by mixing the concentrated HCl with preheated (250 °C, 12 h) KBr and $KBrO_3$ powders. Two $SnCl_2$ solutions of 0.20 and 0.03 g/mL were prepared by dissolving the solid in 1 M HCl and were used for online reduction of Hg during the concentration and isotope measurement steps, respectively. For neutralizing the excess BrCl, a 0.25 g/mL $NH_2OH{\cdot}HCl$ solution was prepared and bubbled for 6 h with Hg-free N_2 to remove trace levels of Hg vapor. The NIST SRM 3133 Hg and UM-Almadén Hg were used as international standards and measured regularly to control the accuracy and quality of isotope analysis (Blum and Bergquist, 2007; Chen et al., 2010), and also served for the method validation coupling with Yellow-Red Soil GBW07405 (National Center for Standard Materials, Beijing, China) (Huang et al., 2015). The NIST SRM 997 thallium solution (20 ng/mL Tl in 3% HNO_3) was used for instrument mass-bias correction. The anion-exchange resin AG-1X4 (200–400 mesh, Bio-Rad®) was used for pre-concentrating Hg from precipitation samples (Chen et al., 2010). All vessels were made either of glass or of Teflon. Borosilicate glass bottles were acid-cleaned by soaking in 10% HNO_3 solution for 24 h followed by rinsing three times with Milli-Q water, then baked for 4 h at 460 °C in a muffle furnace. The vessels in Teflon were cleaned similarly and air dried for 24 h in a laminar fume hood. For rainwater collecting, a 1.2 m × 1.0 m Teflon board (3 mm thick) was deformed into a "U"-type sampler (surface area of ~0.9 m^2) and fixed through four Nylon sticks at 1.5 m above ground. The rainwater

was channeled through the slightly inclined sampler into a 5 L glass beaker. The whole sampler system (Teflon board and beaker) was pre-cleaned by 10% HNO_3 then with bulk Milli-Q water just before each event and had a blank <15 pg ($n = 8$).

2.2. Field setting and sample collection

In this work we investigated the variation of Hg isotope composition, and the relative influence of controlling factors on sequential precipitation samples collected in Guiyang (China). Guiyang is located on the Chinese Yunnan-Guizhou Plateau, an important Hg emission area, where a large amount of coal is consumed by industrial and domestic heating (Fu et al., 2011; Z. Wang et al., 2015). Guiyang has a city population of about 4.7 million in 2013 and a typical subtropical humid monsoon climate (generally from May to October). The annual precipitation depth, temperature and relative humidity (RH) in Guiyang are 1100–1400 mm, 15.3 °C and approximately 77%, respectively (Feng et al., 2011). Recently, the region has been experiencing dramatic urbanization and industrialization with increasing demand for coal and cement (Fu et al., 2011; N. Liu et al., 2011), adding much more Hg to the atmospheric burden.

The sampling site is shown in Fig. S1. The rain samples were collected on an open-air grass field at the Institute of Geochemistry, Chinese Academy of Sciences (IGCAS, 26.35°N, 106.73°E, 1080 m a.s.l.) using the "U"-type Teflon sampler. The rainwater was sequentially collected from three rain events (hereinafter marked as E1, E2 and E3). For comparison, single composite integrated samples (marked as Os, in Table 1) were collected from six other rain events.

2.3. Sample processing

Following collection, the rain water was immediately filtered using a pre-cleaned high borosilicate glass cone-shaped filtration device (2 L) with 0.45 μm mixed cellulose membrane. The blank of the filtration system was 9 pg Hg ($n = 7$). The first ~50 mL of filtered samples was discarded. After filtration, the particles on the membranes were stored frozen at −20 °C, and the filtered water samples were acidified with HCl to 0.1 M, then digested with 0.2 M BrCl and stored at 4 °C. The pre-concentration of Hg filtered from the rain water samples was conducted following the protocol developed by Chen et al. (2010). The pre-concentration method was checked again using NIST SRM 3133 Hg and UM-Almadén Hg, and showed a recovery of 99–101% ($n = 11$) with no Hg isotopic fractionation. Finally, Hg was eluted with 5 ml 0.05% L-cysteine in 0.5 M HNO_3. The Hg elution solution was digested again with BrCl for at least 12 h to consume the residual L-cysteine. Samples were sealed and stored at 4 °C until analysis. The $NH_2OH{\cdot}HCl$ solution was added just before the Hg isotope ratio determination (Chen et al., 2010). The average process blank was average 80 pg ($n = 9$).

For particulate Hg, the freeze-dried particles (bound to the filter membranes) were digested with a fresh mixture of HNO_3-HCl (1:3, V/V) in a water bath (95 °C) for 3 h (Huang et al., 2015). After cooling to ambient temperature, the digested samples were treated with 0.2 M BrCl (5% v/v) for at least 12 h, and then centrifuged at 4000 rpm for 15 min to separate solid residue from the solution. Next, the supernatant was transferred to a pre-cleaned glass vessel and diluted to 20% with Milli-Q water. Finally, the remaining BrCl was neutralized with $NH_2OH{\cdot}HCl$ before the Hg isotope ratio measurement (Huang et al., 2015). The average blank for this digestion was average 30 pg ($n = 7$), negligible compared to Hg mass needed (>5 ng) for isotope measurement.

2.4. Concentration and isotope analysis

Cold vapor atomic fluorescence spectroscopy (CVAFS, Tekran 2500, Tekran® Instruments Corporation, CA) was used to measure filtered Hg concentrations of the precipitation samples following the U.S. EPA

Table 1
Hg concentrations and Hg isotopic composition for rainwater samples of rainfall events in Guiyang, China (the event E1, E2 and E3 are intra-precipitation samples; others events are integrated samples).

ID	Sampling time	Depth/mm	Volume/L	Pre. rate/mm/h	Hg_D/ng/L		$\delta^{202}Hg$/‰		$\Delta^{199}Hg$/‰		$\Delta^{200}Hg$/‰		$\Delta^{201}Hg$/‰		$\delta^{2}H$/‰	$\delta^{18}O$/‰	*d-excess*/‰
					Hg_F	Hg_{PM}	Hg_F	Hg_{PM}	Hg_F	Hg_{PM}	Hg_F	Hg_{PM}	Hg_F	Hg_{PM}			
UM-Almadén ($n = 42$, 2sd)							−0.56 ± 0.12		−0.02 ± 0.07		0.01 ± 0.06		−0.04 ± 0.06				
Event-1 (E1)	2014/3/30–3/31																
E1-R1	21:20–21:45	4.1	3.2	9.90	13.0	12.6	−0.84	−1.07	0.81	0.40	0.10	0.11	0.81	0.42	−5.04	−3.34	21.68
E1-R2	21:45–23:10	2.8	2.2	6.80	12.2	10.9	−0.61	−1.00	0.41	0.19	0.08	0.10	0.44	0.21	−23.43	−4.55	12.97
E1-R3	23:10–03:00	3.7	2.9	0.97	10.9	9.2	−0.44	−0.58	0.53	0.22	0.08	0.08	0.53	0.29	−19.56	−4.08	13.08
Event-2 (E2)	2014/4/05–4/06																
E2-R1	22:15–23:00	3.8	6.0	5.13	31.1	23.7	−2.04	−2.52	0.29	0.20	0.03	0.05	0.24	0.16	−2.85	−3.00	21.15
E2-R2	23:00–24:00	1.9	3.0	1.92	17.7	8.5	−2.00	−2.32	0.26	0.19	0.03	0.04	0.22	0.12	−12.24	−3.71	17.44
E2-R3	00:00–02:00	1.8	2.8	0.90	13.6	5.5	−2.21	−2.38	0.40	0.18	0.03	0.02	0.30	0.15	−11.29	−3.66	17.99
Event-3 (E3)	2014/6/28																
E3-R1	18:25–18:58	8.2	8.0	14.93	8.0	2.9	−1.26	−1.60	0.41	0.02	0.10	0.09	0.29	−0.09	−62.49	−8.60	6.31
E3-R2	18:58–19:10	7.2	7.0	35.93	7.9	1.0	−1.37	−1.50	0.22	0.11	0.08	0.11	0.20	0.03	−68.13	−10.04	12.19
E3-R3	19:10–19:25	7.1	6.9	28.34	6.9	1.3	−1.23	−1.44	0.25	0.04	0.06	0.08	0.24	0.03	−68.27	−9.78	9.97
E3-R4	19:25–19:38	4.0	3.9	18.48	3.9	1.2	−0.97	−1.23	0.32	0.28	0.10	0.16	0.36	0.19	−69.92	−10.27	12.24
Others (Os)																	
Os-R1	2014-3-31 23:00–00:00	2.9	4.5	3.48	11.8	/	−0.25	/	0.81	/	0.13	/	0.73	/	/	/	/
Os-R2	2014-4-01 00:00–03:00	4.1	6.4	1.37	15.6	/	−1.44	/	0.41	/	0.08	/	0.37	/	/	/	/
Os-R3	2014/4/02 00:00–05:00	1.0	0.8	0.20	23.7	/	−0.94	/	0.62	/	0.04	/	0.54	/	/	/	/
Os-R4	2014/4/02 18:00–01:00	0.6	0.9	0.09	9.7	/	−1.20	/	0.52	/	0.03	/	0.42	/	/	/	/
Os-R5	2014/4/07 07:00–09:00	1.0	1.5	0.50	15.8	14.2	−1.07	−0.91	0.65	−0.10	0.05	0.05	0.56	−0.11	/	/	/
Os-R6	2014/4/08 05:00–09:30	1.6	2.5	0.36	8.6	/	−1.22	/	0.44	/	0.05	/	0.34	/	−15.98	−3.98	15.86

Method 1631 (EPA, 2002). Hg concentrations measured on CVAFS and MC-ICP-MS showed no statistic difference ($r^2 = 0.894$; $p < 0.01$) from those measured on MC-ICP-MS after chromatographic pre-concentration (Fig. S2). For the particulate phase Hg, the concentrations and isotopic compositions were determined by MC-ICP-MS. The stable hydrogen and oxygen isotope analysis were completed on a Los Gatos Research liquid water isotope analyzer (LWIA DLT-100, LGR, USA). Final results were expressed in ‰ relative to the Vienna Standard Mean Ocean Water (V-SMOW) value (Craig, 1961), with the measurement accuracy of ±0.5‰ for δ^2H and ±0.2‰ for δ^{18}O.

Hg isotope ratios of both Hg_F and Hg_{PM} were determined by MC-ICP-MS (Nu Instruments Ltd., UK) at the IGCAS, following previously reported methods (Blum and Bergquist, 2007; Chen et al., 2010; Lin et al., 2015). Instrumental bias was corrected using the addition of an internal standard (NIST SRM 997 with $^{205}Tl/^{203}Tl$ ratio of about 2.38714) and sample-standard bracketing (SSB). Analysis was run at 1–3 ng/mL Hg, depending on available Hg mass (sample size), and standard concentrations were matched to that of samples (within 5%). The ^{202}Hg signal was approximately 2 V for 2 ng/mL Hg. The MDF Hg isotopes ratios were defined by the following equation (δ^xHg in ‰) (Blum and Bergquist, 2007):

$$\delta^{x}\mathrm{Hg} = \left(\frac{\left(\frac{^{x}\mathrm{Hg}}{^{198}\mathrm{Hg}}\right)_{\mathrm{sample}}}{\left(\frac{^{x}\mathrm{Hg}}{^{198}\mathrm{Hg}}\right)_{\mathrm{std}}} - 1 \right) \times 1000 \quad (1)$$

where x = 199, 200, 201, 202, "std" was NIST SRM 3133 Hg solution. MIF of Hg isotopes was defined as the difference between the measured δ^xHg and the theoretically predicted MDF, and was expressed as capital delta notation according to following equations (Blum and Bergquist, 2007):

$$\Delta^{199}\mathrm{Hg} = \delta^{199}\mathrm{Hg} - 0.252 \times \delta^{202}\mathrm{Hg} \quad (2)$$

$$\Delta^{200}\mathrm{Hg} = \delta^{200}\mathrm{Hg} - 0.502 \times \delta^{202}\mathrm{Hg} \quad (3)$$

$$\Delta^{201}\mathrm{Hg} = \delta^{201}\mathrm{Hg} - 0.752 \times \delta^{202}\mathrm{Hg} \quad (4)$$

Our repeated measurements of the standard UM-Almadén Hg were in accordance with the previous studies (Blum and Bergquist, 2007) and gave long-term average values of −0.56 ± 0.12‰, −0.02 ± 0.07‰, 0.01 ± 0.06‰ and −0.04 ± 0.06‰ ($n = 42$, 2sd) for δ^{202}Hg, Δ^{199}Hg, Δ^{200}Hg and Δ^{201}Hg, respectively. The 2sd values of UM-Almadén Hg measurement were considered as the typical external uncertainties for our samples that were measured only once due to the limited sample volume and Hg mass.

2.5. Meteorological data analyses

In addition to Hg concentrations and isotope ratios, we explored the meteorological data from the three rainfall events. Surface meteorological data including the synoptic scale meteorological evaluation (frontal systems, surface-wind directions and speed, temperature, radiation intensity and relative humidity, etc.) were obtained from the Meteorological Information Center of Guizhou, a national weather observatory located approximately 500 m north of the rain sampling site. The cloud-top heights were where the relative air humidity was lower than 85% detected by a sensor equipped on a rising weather balloon at 7 am and 5 pm (local time, LT) every day. HYSPLIT back trajectories (available online: http://ready.arl.noaa.gov/HYSPLIT.php) were calculated every 6 h starting at different heights (Chen et al., 2012; Jaffe et al., 2005). The heights of 500 m and 1000 m above ground level (AGL) were particularly useful for modeling the vertical movements of air masses in the atmosphere boundary layer (ABL, generally <1000 m), where pollutants released by human activities mainly resided and accumulated. The height of lower than the cloud-top was used for calculating the pathway of the long-term transported air masses.

3. Results

Table 1 showed the data set of sampling information, Hg concentrations and isotopic compositions of all rain waters in Guiyang. Except for four samples of E3 collected in the late afternoon during the June monsoon period, the other rainwaters were sampled in the night of non-monsoon season (October to April) when the ABL is relatively shallow (Fu et al., 2011). The special sampling period and precipitation depth were also gathered in Table 1. Cloud top (see discussion below) and the meteorological data were in Table S1. The measured stable oxygen and hydrogen isotopes in rainwater converge on the reference line defined by the data from the Global Network of Isotopes in Precipitation (GNIP) station in Guiyang (Fig. S3).

3.1. Concentration and isotopic composition of filtered Hg in precipitation

Filtered Hg concentrations in all wet precipitation samples varied from 3.9 ng/L to 31.1 ng/L (average 13.1 ng/L), and was consistent with the data previously reported in this region (J. Liu et al., 2011; Z. Wang et al., 2015) and some North America regions (such as Illinois and Florida) (Lynam et al., 2014; Sherman et al., 2012). However, the values were lower than those of Chinese megacities, such as Shanghai (>40 ng/L) (Zhang et al., 2010), and higher than the background regions in China (average < 3 ng/L) (Huang et al., 2012; Zhou et al., 2013).

Isotopically, Hg_F in precipitation generally displayed negative δ^{202}Hg of −2.21‰ to −0.25‰, with the highest value of −0.25‰ for Os-R1, and the lowest value of −2.21‰ for E2–R3 (Figs. 1 and 2, Table 1). All these δ^{202}Hg values were encompassed by those reported in our previous study for the same place (Z. Wang et al., 2015). The studies from other places worldwide have also reported negative δ^{202}Hg, such as Lhasa in China (−0.80‰ to −0.42‰) (Yuan et al., 2015), and Peterborough (−1.59‰ to −0.02‰), Florida (−4.37‰ to 0.21‰) and the Great Lake region (−1.13‰ to 0.18‰) in the North America (Chen et al., 2012; Gratz et al., 2010; Sherman et al., 2012, 2015). In contrast to δ^{202}Hg used as an indicator of MDF, Hg_F had significantly positive $\Delta^{199}Hg_F$, ranging from 0.22‰ to 0.81‰ (with average 0.46‰), similar to those reported for precipitation from Lhasa, China (0.38‰ to 0.76‰) (Yuan et al., 2015), and in the North America (−0.87‰ to 1.13‰) (Chen et al., 2012; Gratz et al., 2010; Sherman et al., 2012, 2015). Similar to data reported in previous studies (Chen et al., 2012; Gratz et al., 2010; Sherman et al., 2012; Z. Wang et al., 2015; Yuan et al., 2015), Δ^{199}Hg and Δ^{201}Hg of the filtered Hg plot along the 1:1 line, similar to that defined by Hg(II) photo-reduction (Fig. 3). Slightly positive Δ^{200}Hg (from 0.03‰ to 0.13‰, average 0.07 ± 0.07‰, 2sd) was detected in all Hg_F of precipitation samples.

3.2. Hg concentration and isotopic composition in the particulate phase

Particles in the E1 samples showed similar Hg concentrations (average 10.9 ng/L) to those of Hg_F within the same sample; however, E2 and E3 particles were lower (from 5.5 to 23.7 ng/L for E2 and from 1.0 to 2.9 ng/L for E3) (Table 1; Fig. 1). Thus, total Hg concentrations (Hg_T, the sum of Hg_F and Hg_{PM}) ranged from 5.1–54.8 ng/L for all samples, with the average value of 21.1 ng/L. All precipitation samples displayed a decrease of Hg concentrations (Hg_F, Hg_{PM} and Hg_T) with precipitation depth (Fig. S4), similar to previous studies (Sherman et al., 2012; White et al., 2013). A general phenomenon was that, for all samples, the total Hg concentrations (and Hg_F) decreased progressively from the beginning to the end of each precipitation event (Fig. 1).

All Hg_{PM} displayed a δ^{202}Hg range from −2.52‰ (E2-R1) to −0.58‰ (E1-R3), with an average value of −1.51‰ (Table 1). Except for the integrated samples Os-R5 (δ^{202}Hg of −0.91‰), all Hg_{PM} has more negative δ^{202}Hg than those of Hg_F from the same samples. Though most Hg_{PM} (except for Os-R5 with a negative value of −0.10‰) displayed positive Δ^{199}Hg (from −0.10‰ to 0.40‰, average of 0.16‰), they were comparatively lower than those of Hg_F (Fig. S5). Similar to Hg_F, all Hg_{PM} data

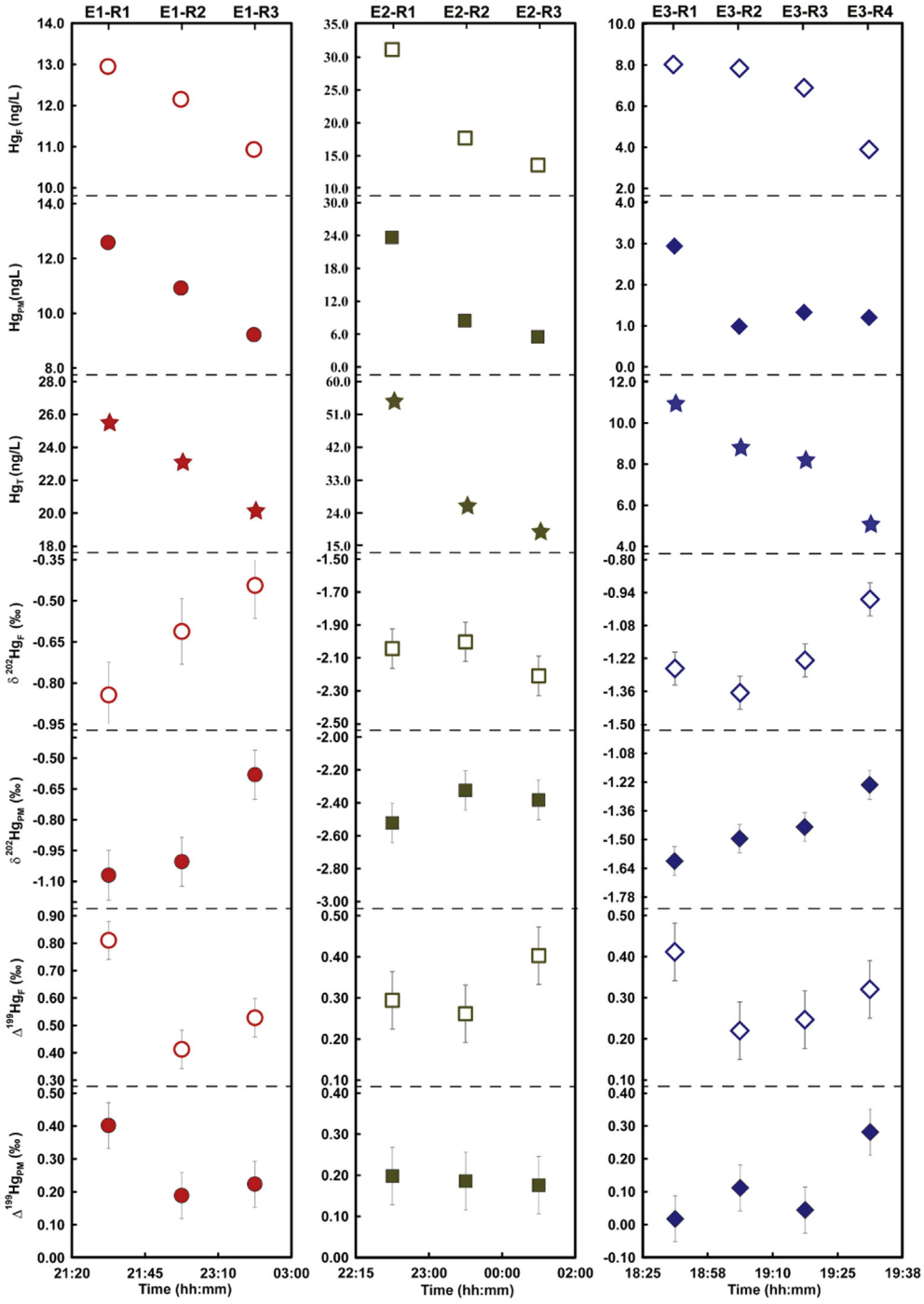

Fig. 1. Stacked graphs showing the variation of Hg concentrations, $\delta^{202}Hg_F$, $\delta^{202}Hg_{PM}$, $\Delta^{199}Hg_F$ and $\Delta^{199}Hg_{PM}$ in the three rainfall events with sampling time.

points were plotted along the line $\Delta^{199}Hg/\Delta^{201}Hg = 1$ (Fig. 3), and were characterized by slightly positive $\Delta^{200}Hg$ (from 0.02‰ to 0.16‰, average 0.08 ± 0.08‰, 2sd).

4. Discussion

4.1. Potential factors controlling the variation of Hg isotopes

Previous studies showed that the atmospheric processes that occurred in the local ABL would have a limited effect on Hg isotopes (Chen et al., 2012; Demers et al., 2015; Gratz et al., 2010; Sherman et al., 2012; Z. Wang et al., 2015). This would also hold for this study. In fact, the $\Delta^{199}Hg/\Delta^{201}Hg$ ratio close to 1 would suggest that the odd-MIF of Hg in Guiyang precipitation has a photo-reduction origin. Although the occurrence of pervasive atmospheric Hg oxidation in Guiyang ABL remained unclear, the fact that all samples showed much lower $\Delta^{199}Hg/\Delta^{201}Hg$ (about 1.0) than that reported for gas-phase oxidation of GEM by halogen atoms (between 1.64 and 1.89) (Sun et al., 2016) probably indicated the limited effect of this process. In addition, isotopic fractionation triggered by adsorption (Wiederhold et al., 2010) and diffusion (Koster van Groos et al., 2013) would only result in slight odd-MIF (generally <0.10‰). Therefore, the variation of Hg isotopes, especially the significant positive odd-MIF in our sequential rain samples, should be derived from different Hg sources. Such conclusion was obtained in most previous studies of Hg systematics in precipitation (Chen et al., 2012; Demers et al., 2013; Donovan et al., 2013; Gratz et al., 2010;

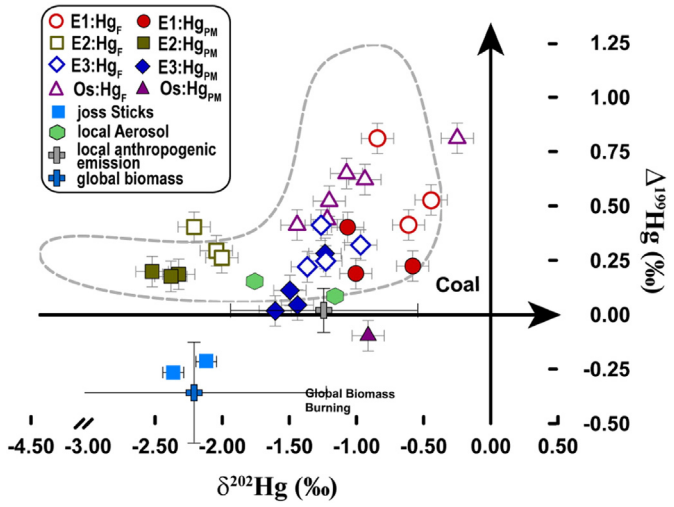

Fig. 2. Relationship between odd-MIF and MDF of Hg isotopes in precipitation. The variation range of Hg isotopic data for precipitation reported in the previous study this region (gray dash line, Z. Wang et al., 2015), local anthropogenic emissions (average ± 1sd, including coal combustion and cement plant emission, Biswas et al., 2008; Sun et al., 2014; Yin et al., 2014), biomass worldwide (average ± 1sd, Das et al., 2015; Demers et al., 2013; Tsui et al., 2012; Yin et al., 2013; Yu et al., 2016) and local aerosols (Huang et al., 2015) were also given.

Sherman et al., 2012, 2015; Z. Wang et al., 2015; Yuan et al., 2015). Our study of precipitation in an individual rainfall event from the Lhasa City on the Tibetan Plateau showed that contributions of different sources could result in large variations of both δ^{202}Hg and Δ^{199}Hg, too (Yuan et al., 2015). Here, we tested if changes of source contributions could eventually trigger also variation of Hg isotopic composition in sequential rainfall samples in Guiyang, by coupling the meteorological data with Hg, O and H isotope ratios, especially *d-excess* (*d-excess* $= \delta^2H - 8 \times \delta^{18}O$). The *d-excess* was largely controlled by temperature and relative humidity and thus can used to trace the moisture's source (Keil et al., 2010), with for example the low *d-excess* value for marine evaporation moisture, whereas high values for moisture derived from in-land dry areas (Keil et al., 2010).

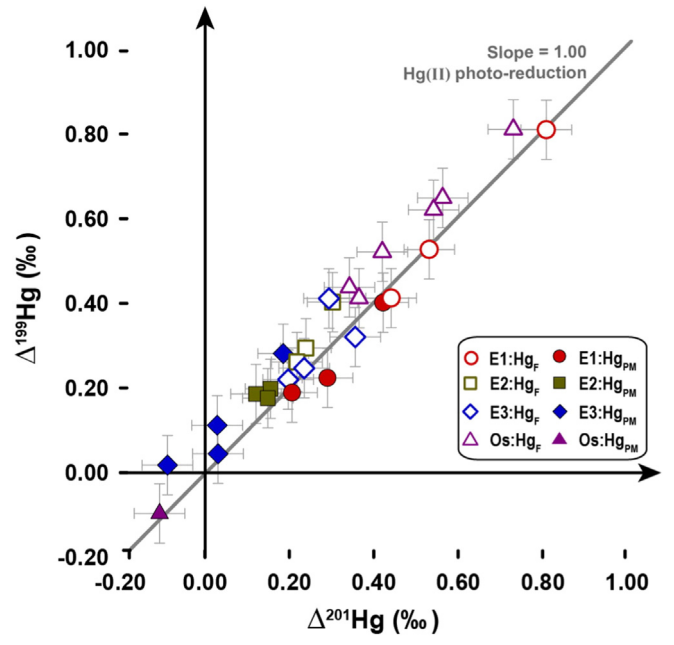

Fig. 3. Odd-MIF of Hg isotopes in all precipitation samples.

4.1.1. Local anthropogenic Hg contribution

Atmospheric precipitation Hg could be significantly impacted by local anthropogenic emission. Previous literature has reported the distribution of industrial Hg emitters in Guiyang (Fu et al., 2011; Zhang et al., 2015). Coal fire power plants (CFPPs) and cement plants are dominant point sources of the region, together with some non-ferrous metal smelting and other industrial factories (Z. Wang et al., 2015). It's worth mentioning that >90% of Hg in raw materials consumed by cement plants are emitted and accumulated in ABL, with major species as Hg(II) that could account for 61%–91% of the total Hg in flue gas (Wang et al., 2014; Z. Wang et al., 2015). This locally released Hg(II) in ABL could have an impact on Hg budget in wet deposition (Fu et al., 2011; Zhang et al., 2015), since it could be easily scavenged into rain water droplets or particles and scavenged below-cloud (Huang et al., 2013; Poissant and Pilote, 1998; Sherman et al., 2012; White et al., 2013; Yuan et al., 2015). Thus, the relatively higher Hg content (compared to the background atmosphere), especially that found at the beginning of precipitation events, could be from local source contribution.

Hydrogen and oxygen isotopic data of rain samples further confirmed the important contribution from local emitted Hg. First, the relatively higher $\delta^{18}O$ and *d-excess* in E1 and E2 indicated a provenance of inland, rather than an oceanic origin (e.g. South China Sea through southeast Asian monsoon or Indian Sea through western monsoon, respectively) (Celle-Jeanton et al., 2004). NOAA-HYSPLIT back-trajectory model also showed that the air mass (below ABL) had a relative long residence time on land before arriving in Guiyang. Moreover, the similarity of MDF Hg isotope ratios between local emission sources (e.g. CFPPs and cement plants, −1.46‰ ~ −1.33‰) and rainfall samples (especially E1 and E3) also confirmed the strong anthropogenic contribution, as discussed in previous studies (Sun et al., 2014; Z. Wang et al., 2015). However, the very high $\Delta^{199}Hg_F$ in some Guiyang rain samples (E1-R1 and Os-R1) cannot be explained by local Hg emission that had close to zero odd-MIF (Sun et al., 2014; Z. Wang et al., 2015), another end member of long-range transportation, which usually has higher $\Delta^{199}Hg_F$ (Chen et al., 2012; Demers et al., 2015; Z. Wang et al., 2015; Yuan et al., 2015), is needed to explain all data distribution.

4.1.2. Long-range transport Hg

Long-range transport could also be important sources to precipitation Hg in Guiyang. This Hg may be derived from both natural and anthropogenic sources and be derived from the free troposphere. For example, previous research showed that up to 60% of Hg in rainwater deposited to the surface in western US originated from the upper atmosphere (>2 km, above ABL) (Gratz et al., 2015; Nair et al., 2013; Weiss-Penzias et al., 2009). Long-range transported Hg has been generally characterized by higher Δ^{199}Hg values than local emissions (Chen et al., 2012; Demers et al., 2015; Z. Wang et al., 2015; Yuan et al., 2015). This Hg could be leached by in-cloud scavenging, which might result in more positive odd-MIF in precipitation samples. In March and April, Guiyang region was dominated by western wind, while the rainy season from May to September is mainly controlled by the Southeast Asia monsoon, indicating westerly (Tibetan plateau) and southeastern contribution as possible long-term sources to Hg. In fact, E3 samples had relatively lower $\delta^{18}O$, which could result from gradual rainout during long-distance transportation, and *d-excess* values, also confirming the contribution of the long-range transported moisture (Dansgaard, 1964; Munksgaard et al., 2012). The odd-MIF (average $\Delta^{199}Hg = 0.83 \pm 0.60$‰, 2sd) in Guiyang rain samples in the dry season (from October to April) was more positive than in the wet season (average $\Delta^{199}Hg = 0.44 \pm 0.33$‰, 2sd) which might result from the strong contribution of the long-range transport Hg from the west (having more positive Δ^{199}Hg values) (Z. Wang et al., 2015). Furthermore, the NOAA-HYSPLIT calculation above ABL confirmed that the Hg budget could be influenced by air masses derived from long distance, even as far as from northern India or Southeast Asia, as demonstrated by our previous study (Z. Wang et al., 2015).

4.2. Isotopic composition of filtered Hg in rainwater

In the following, we mainly discussed the factors triggering the isotopic variation of Hg_F in sequential samples of three individual rainfall events (E1, E2 and E3); That is the local meteorological or source changes that could play an important role in the variations of Hg concentration, and even isotopic composition during the intra-precipitation. Previous work showed that even a small change in surface wind direction and speed could result in significant change of Hg concentrations in precipitation (White et al., 2013). Thus, one could expect that variable contributions from different sources with regard to the changing meteorological condition would induce significant Hg isotope variation even in a relative short period (Yuan et al., 2015).

4.2.1. Event 1

Rainfall event 1 locally started at 21:20 30th March and ended at 03:00 31st March (+8 G.M.T.), 2014. Rain waters were collected in dry season (March and April) in Guiyang. Though Hg_F concentrations of all three events decreased progressively with time, the three E1 samples (E1-R1, E1-R2 and E1-R3) showed the smallest variation range (from 13.0 to 10.9 ng/L) compared to the two others events (E2 and E3) (Fig. 1). However, amongst these three events, E1 samples displayed the largest variation of both MDF and odd-MIF, with $\delta^{202}Hg_F$ values increasing with time (from −0.84‰ for E1-R1 to −0.44‰ for E1-R3), while the odd-MIF values decreased.

Previous studies showed that, though long-range transported and locally emitted Hg both would possess large variation range of MDF (from −4.37‰ to 0.21‰), the long-range transported Hg had generally higher odd-MIF compared to the local anthropogenic emission (Chen et al., 2012; Gratz et al., 2010; Sherman et al., 2015; Sherman et al., 2012; Z. Wang et al., 2015; Yuan et al., 2015). Of the three samples, the first rainwater (E1-R1) was characterized by the most positive odd-MIF. According to the meteorological information, a stationary cold front covered Guiyang City during the sampling period. The air mass back trajectory calculation showed that the warm and humid air arrived at moderately high altitude (below 2600 a.s.l., Fig. S6). The rainfall of E1 event was associated with movement of a cold front across the area, with 10.7 mm depth in about 6 h (from 21:00, 30 March, LT to 03:00 next day). The incorporation of long-range transported Hg with higher $\Delta^{199}Hg$ (up to 1.57‰ from western monsoon; Z. Wang et al., 2015) by water droplets condensed intensively at the beginning of E1 event which explained the most positive odd-MIF (and high Hg content) found in the E1-R1 sample. The relatively high $\delta^{18}O$ values (between −4.55‰ to −3.34‰, Table 1) and *d-excess* (21.68‰) also suggested a large contribution of long-range transported air mass at the beginning of the E1 event (Celle-Jeanton et al., 2004). Although local emission by human typically has higher concentration than long-range transport (Fu et al., 2011), the fact that rainfall events occurred before the E1 event would have leached much more locally emitted Hg, leading to a decrease of anthropogenic Hg in ABL (Seo et al., 2012). This would result in removal of locally emitted Hg with lower $\Delta^{199}Hg$. Another explanation could be a downward humidity gradient in-between the warm and humid cloud on the top and the dry and cold air mass beneath would result in possible evaporation of water vapors during the fall of droplets (Table S1), which again favored the slightly higher Hg concentration for the first sample E1-R1.

At the middle and end of the rainfall event (samples E1-R2 and E1-R3), the stationary front became stronger, the shear line moved southward and the precipitation rate decreased with time. A cold air mass moved in (Table S1), and Hg concentration and odd-MIF of samples E1-R2 and E1-R3 decreased, but $\delta^{202}Hg$ increased (Fig. 1 and Table 1). The Hg concentration decrease could be due to scavenging of Hg from the air during initial rainfall (Yuan et al., 2015; Sherman et al., 2012). This also resulted in removal of the component of Hg derived from long range transport and decrease of $\Delta^{199}Hg$ caused by the increasing contribution of local emission which occupied higher proportion than long range transport Hg and generally displayed lower odd-MIF (Z. Wang et al., 2015). Precipitation at the end of the event scavenged local Hg resulting in lower odd-MIF. In addition, the long distance that water droplets traveled (higher cloud altitude of 5800 m a.s.l.) down to surface allowed for incorporating much more anthropogenic Hg by below-cloud scavenging, explaining the $\delta^{202}Hg$ variation in the case of continuous supply of industrial emission. In fact, local emission may have relatively heavier isotopes (^{202}Hg) than those of long-range transportation (Chen et al., 2012; Gratz et al., 2010; Yuan et al., 2015). For example, higher $\delta^{202}Hg$ in local emission was observed relative to the long-range transportation Hg in North America (Chen et al., 2012). Finally, the quasi-constant high $\delta^{18}O$ values (between −4.55‰ to −3.34‰, Table 1) indicated a continuous supply of long-range transportations with droplets in clouds for the E1 event (Celle-Jeanton et al., 2004). This might explain the relatively higher $\Delta^{199}Hg$ determined in all three E1 samples compared to samples of two other events (Table 1, Fig. 2).

4.2.2. Event 2

The rainfall event E2 started at 22:15 5th April and ended at 02:00 6th April (+8 G.M.T.), 2014. In three samples of E2, the Hg_F concentrations (13.6 to 31.1 ng/L) were much higher than that of E1 and E3, and decreased progressively with time. These three samples displayed quasi-constant $\delta^{202}Hg$ values (from −2.21‰ to −2.00‰) and odd-MIF ($\Delta^{199}Hg$ from 0.26‰ to 0.40‰), both relatively lower than the samples of E1 and E3.

Mercury in samples of event E2 could not be directly derived from local sources or long-range transport, since the local anthropogenic emission ($\delta^{202}Hg$ of −1.46‰ to −1.33‰, $\Delta^{199}Hg$ close to 0) from CFPPs and cement plants and long-range transported Hg (positive $\Delta^{199}Hg$) showed very different MDF and odd-MIF, respectively (Z. Wang et al., 2015). Besides, much more positive $\delta^{18}O$ (−3.71‰ to −3.00‰) values and high *d-excess* (17.44‰ to 21.15‰) could suggest an inland origin of atmospheric moisture. The fact that all E2 samples contained much higher Hg concentration would thus likely suggest another contributing source.

The sampling day, 5 April, was the traditional Tomb Sweeping Day in China, when every family would commemorate and honor recently deceased relatives or distant ancestors, by burning incense (both joss sticks and joss paper, with joss paper taking the large proportions) (Fang et al., 2002). The incense was mainly made from plants, such as bark, roots, and other auxiliary materials (Wang et al., 2007). The combustion of these materials could emit a large amount of Hg into atmosphere, in the form of either GEM or oxide form Hg(II) (Nzihou and Stanmore, 2013; Shen et al., 2017), being a potential source to Hg in all E2 event.

Isotopically, all E2 samples displayed $\delta^{202}Hg$ value of −2.21‰ to −2.00‰, consistent with data prior reported for biomass samples (average $\delta^{202}Hg = -2.22 \pm 2.01$‰, 2sd, $n = 169$) (Das et al., 2015; Demers et al., 2013; Tsui et al., 2012; Yin et al., 2013; Yu et al., 2016). Thus, the biomass (incense) combustion may be a potential contributor. Although the joss sticks from Guiyang showed the similar $\delta^{202}Hg$ (average -2.24 ± 0.37‰, $n = 2$, 2sd) with vegetation samples (Das et al., 2015; Demers et al., 2013; Tsui et al., 2012; Yin et al., 2013; Yu et al., 2016) and E2 rain samples (Tables 1 and 2), burning of the joss sticks could not explain the high Hg concentrations (thus large amount) of event E2, as they represented very smaller proportion of incense. Moreover, the negative $\Delta^{199}Hg$ value of the joss sticks ($\Delta^{199}Hg = -0.24 \pm 0.06$‰, $n = 2$, 2sd) could not endorse the positive odd-MIF of event E2 either. Thus, the combustion of joss papers, rather than joss sticks, would be the dominant contributor to Hg in E2 event.

In order to verify the exact contribution of Hg released from the joss paper, we conducted a simple combustion experiment of joss paper in an open system (see detail in SI). The average Hg isotopic ratios of raw joss papers and its ash residue ($n = 4$) were -0.70 ± 0.12‰ and 0.11 ± 0.33‰ for $\delta^{202}Hg$ (2sd) and 0.07 ± 0.06‰ and -0.05 ± 0.03‰ for $\Delta^{199}Hg$ (2sd), respectively. Unfortunately, the mass balance (and thus the isotopic composition of emitted Hg subspecies) could not be

Table 2
Hg isotope results of the simple joss paper burning experiment and the summary of Hg isotope data previously reported for biomass, coals and cement plant emission.

Samples	Samples ID	δ^{202}Hg (‰)	Δ^{199}Hg (‰)	Δ^{200}Hg (‰)	Δ^{201}Hg (‰)
Joss stick	GI-1	−2.12	−0.22	0.12	−0.21
	GI-2	−2.36	−0.27	0.02	−0.15
Joss paper	PAH-1	−0.69	0.03	−0.01	−0.08
	PAH-2	−0.78	0.05	0.07	−0.08
	PBH-1	−0.69	0.01	0.04	−0.07
	PBH-2	−0.64	0.19	0.19	0.13
Joss paper ash	AH-1	−0.25	−0.07	0.07	−0.07
	AH-2	−0.23	−0.05	0.06	−0.05
	AH-3	−0.07	−0.06	0.07	−0.11
	AH-4	0.10	−0.04	0.03	−0.07
Biomass (2sd, $n = 30$)[a]		−2.22 ± 2.01	−0.37 ± 0.45	0.01 ± 0.15	−0.40 ± 0.47
Coal from Guizhou (2sd $n = 14$)[b]		−1.27 ± 1.35	0.03 ± 0.19	0.01 ± 0.08	−0.01 ± 0.14
Cement plant emission[c]		−1.33	−0.06	/	−0.05

[a] (Das et al., 2015; Demers et al., 2013; Tsui et al., 2012; Yin et al., 2013; Yu et al., 2016).
[b] (Biswas et al., 2008; Sun et al., 2014; Yin et al., 2014).
[c] (Z. Wang et al., 2015).

calculated due to the lack of the emitted material mass and instantaneous weather condition for the combustion experiment. However, according to the Hg isotopic composition of above raw joss paper and its ash residue, the isotopic composition of bulk emitted Hg mixture (i.e. GEM, $Hg(II)_D$ and PBM) could be approximately estimated, and should be characterized by much lower δ^{202}Hg and similar or slightly higher Δ^{199}Hg (Fig. 4). Previous work on coal combustion reported that the oxidized forms of emitted Hg ($Hg(II)_D$ and PBM) were generally depleted in heavier Hg isotopes relative to GEM (Sun et al., 2014). If this also holds for joss paper burning, the $Hg(II)_D$ and PBM of emitted Hg should be characterized by even more negative MDF. These Hg isotope data (both MDF and odd-MIF) of joss paper burning emission were consistent with those determined in our event E2 samples. Therefore, the emitted Hg(II) from the incense burning in Tomb Sweeping Day contributed to the observed Hg concentrations in event E2 rain waters. Though the contribution of spring biomass burning in the Indo-China Peninsula through trans-boundary transport could not be excluded (X. Wang et al., 2015), given the dominant western wind of the sampling period for Guiyang City, this contribution would be limited.

It should be mentioned here that the raw joss paper displayed relatively higher Δ^{199}Hg values (average 0.07 ± 0.16‰, 2sd, $n = 4$) compared to the odd-MIF data reported for biomass materials worldwide (average −0.37 ± 0.45‰, 2sd, $n = 169$) (Das et al., 2015; Demers et al., 2013; Tsui et al., 2012; Yin et al., 2013; Yu et al., 2016). Though the exact mechanism inducing this difference remained unknown, the fact that some auxiliary materials (i.e. resins, essential oils and synthetic substitute chemicals) (Jetter et al., 2002) would be added during the Joss paper production could be a possible cause.

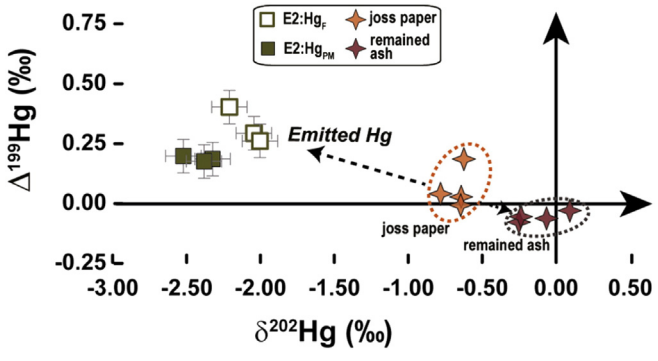

Fig. 4. Figure illustrating the result of the simple incense paper burning experiment. The relative lower Δ^{199}Hg but higher δ^{202}Hg in the remained ash compared to the bulk incense paper would imply contrasting Hg isotopic compositions (higher Δ^{199}Hg while lower δ^{202}Hg) for the emitted Hg, which could be largely captured by local precipitation.

Unlike the two other events E1 and E3, E2 samples displayed the lowest MDF and odd-MIF variation (Table 1 and Fig. 1). This could be probably explained by the strong contribution of local incense combustion in this special day. The incense burning scenario lasted for several hours in the evening, and the large emission of Hg (mainly Hg(II)) that accumulated in the ABL layer could be readily scavenged into water droplets and deposited through rainfall to the surface. The large input of Hg from the local incense combustion reacted as the dominant source, and thus totally buffered the contribution of other sources, especially the long-range transport with low Hg content, explaining the quasi-constant Hg isotope ratios. The highest Hg concentrations determined in all three E2 samples supports the suggestion that incense combustion was the dominant Hg source. Accordingly, other rain samples (Os-R1 to Os-R6; Table 1) collected before and after this event had more positive odd-MIF, confirming the "buffer effect" derived from the incense combustion, which further verified the above hypothesis in return. During the whole E2 event, the decrease of Hg_F to the end might imply a decline of this local contribution, due to for example the concomitant ease of incense combustion activity.

4.2.3. Event 3

The event 3 locally started at 18:25 and ended at 19:38 28th June (+8 G.M.T.), 2014, during the monsoon period in Guiyang. This was a relatively heavy rain with the precipitation depth up to 26.5 mm in only 73 min, and thus much greater precipitation rates (between 14.9 to 35.9 mm/h) than the other rainfall events (<10.0 mm/h). In spite of the lower Hg concentration in this event likely caused by the frequent wet scavenging in the rainy season, the Hg deposition flux of E3 (187 ng/m^2) was comparable to E1 (129 ng/m^2) and E2 (178 ng/m^2), due to the large amount of rainwater. Hg concentrations also decreased progressively similarly to the above two events. The four E3 samples displayed small variation of both MDF and odd-MIF, with negative $\delta^{202}Hg_F$ values (from −1.37‰ to −0.97‰) but positive $\Delta^{199}Hg_F$ (from 0.22‰ to 0.41‰). From the beginning to the end of E3 rainfall, the odd-MIF showed a general decrease as E1, while δ^{202}Hg increased.

This similarity of δ^{202}Hg between rain samples and local Hg sources (−1.46‰ ~− 1.33‰, Z. Wang et al., 2015) suggested the contribution of local Hg emission to this event as well. However, the local anthropogenic source generally characterized by insignificant odd-MIF could not explain the positive $\Delta^{199}Hg_F$ in event E3. Thus, another contribution with higher Δ^{199}Hg was needed to explain this result. E3 samples were collected during the Southeast Asian monsoon season (June) in Guiyang, the more negative δ^{18}O and lower *d-excess* (weighted average −9.56‰ and 9.78‰, respectively) might indicate a marine provenance, such as the Southern Ocean for the atmospheric moisture (Munksgaard et al., 2012). Thus the southern long-term transport with higher odd-MIF would be a possible source. This was also confirmed by the HYSPLIT

back trajectory calculation (Fig. S8). Our previous study on Guiyang precipitation captured this southern long-range contribution too (Z. Wang et al., 2015). Therefore, both local Hg emission and southern long-range transport could both contribute to Hg in event E3 rain.

The E3 samples were collected during the Southeast Asian monsoon, when southern warm and wet air dominated the Guiyang region. Similarly to E1, the rainfall of event E3 was a strong frontal system with a large number of warm droplets on the top of the locally derived cool air mass. Considering the large amount of rainwater (26.5 mm precipitation in only 73 min), the relatively lower Hg content for all E3 samples would indicate a dilution effect, which further lead to the decrease of Hg concentration with time (Fig. 1). At the beginning stage, the southern long-range transported warm droplets would largely condense on the warm-cool front in a very short time, promoting the large or even dominated contribution of long-range transported Hg. This explained the relatively higher Δ^{199}Hg of 0.41‰ for the first E3-R1 sample. Thereafter, the proportion of anthropogenic Hg would increase, along with the continuous emission of anthropogenic Hg (with higher $\delta^{202}Hg_F$ but lower $\Delta^{199}Hg_F$; see Z. Wang et al., 2015) into AGL, which would induce an increase in rainwater of $\delta^{202}Hg_F$, but a decrease of odd-MIF at the middle and later stages of E3.

In conclusion, in addition to the general local anthropogenic sources (i.e. CFPPs and cement plants) and western and southern long-range transport previously determined by our group (Z. Wang et al., 2015), the specific incense combustion on the traditional Chinese Tomb Sweeping Day was also an important occasional contributing source, especially for Hg in the E2 rainfall samples. The different Hg isotope variations of these three independent rainfall events likely resulted from the variable contributions of various sources with different isotopic signatures, also influenced by change of meteorological conditions. This change might be achieved in a very short time period (hours or even minutes), resulting in a large variation of Hg isotopic composition during the single rainfall event. Our results also showed that rainfall Hg was indeed very sensitive to the change of source contribution, as the Hg isotopic signature of the occasional incense burning could be immediately captured in local precipitation.

4.3. Isotopic composition of particulate hg in rainwater

This study reported, for the first time, Hg isotopic composition of particles concomitantly collected and separated from precipitation samples. Although the particulate Hg (Hg_{PM}) had Hg concentrations (average 8.3 ng/L) relatively lower than the filtered Hg (Hg_F) of the same sample, its average proportion to THg was 33.8% (ranging from 11.2% to 49.3%), demonstrating that a significant amount of Hg in precipitation was in particulate form. The average concentration value was comparable with precipitation of most urban areas globally (Huang et al., 2013; Schroeder and Munthe, 1998), in contrast to the arid regions such as Tibetan Plateau where Hg_{PM} made up > 70% of the precipitation THg on average (Huang et al., 2012, 2013). In general, Hg_{PM} was characterized by Hg isotopic compositions statistically different ($p < 0.01$ for both δ^{202}Hg and Δ^{199}Hg) from the filtered phase, with $\delta^{202}Hg_{PM}$ (average -1.51 ± 1.30‰, 2sd) and $\Delta^{199}Hg_{PM}$ (average 0.16 ± 0.27‰, 2sd) lower than those of Hg_F (average $\delta^{202}Hg = -1.19 \pm 1.10$‰, $\Delta^{199}Hg = 0.46 \pm 0.37$‰, 2sd, respectively). These values were consistent with the data previously reported for the PBM in Guiyang (average $\delta^{202}Hg = -0.85 \pm 1.10$‰ and average $\Delta^{199}Hg = 0.04 \pm 0.11$‰, 2sd, $n = 41$) (Huang et al., 2015; Yu et al., 2016), except for event E2. Large variations of both MDF and odd-MIF of Hg isotopes were also found for the single rain events with the largest δ^{202}Hg variation of 0.49‰ for E1, and Δ^{199}Hg of 0.26‰ for E3.

Mercury would exist mainly in Hg(II) form in both filtered and particulate phases in precipitation. As found for the filtered phase, the Hg isotope variation of rainwater particles would also be controlled by variable source contribution. Although the isotope exchange between Hg_{PM} and Hg_F could also lead to Hg isotopic change in particles, which needs to be further studied, the high distribution coefficient (about 10^5) between Hg_{PM} and Hg_F would suggest the limited impact of filtered phase on particulate Hg isotopes. Similar result was obtained for lake water Hg isotope systematics (Chen et al., 2016). This was further confirmed by the inconsistent variations of MDF and odd-MIF between Hg_F and Hg_{PM} during the single one event (Fig. 1). Thus, variable source contribution would be the main cause explaining both MDF and odd-MIF variations in rainwater Hg_{PM}.

The Hg_{PM} isotopic ratios determined in this study were consistent with those previous reported in Guiyang (Huang et al., 2015; Yu et al., 2016). Considering our data and prior studies, both local anthropogenic sources (i.e. CFPPs and cement plants) and the long-range transport (aerosols) could contribute to the Hg_{PM} in precipitation, as demonstrated by Hg_F phase. The similarity of Hg isotopic composition between rainwater Hg_{PM} and anthropogenic emission (Sun et al., 2014; Z. Wang et al., 2015) confirmed the local source input, while the relatively higher odd-MIF in especially event E1 particles would require a long-range contribution with generally higher Δ^{199}Hg (Chen et al., 2012; Huang et al., 2015), as a result of long-distance transport (Clarke et al., 2013) and the simultaneously occurred photo-reduction (Landis et al., 2014; Tong et al., 2014; Zheng and Hintelmann, 2010). The relatively lower values of Hg_{PM} for both MDF and odd-MIF, as compared to Hg_F of samples (Table 1 and Fig. 1) suggested a larger contribution from anthropogenic particles (Seo et al., 2012). Moreover, similar to Hg_F of E2 event, particles emitted from incense burning on the Tomb Sweeping Day could largely impact isotopic signature of E2 Hg_{PM}. Soil particles that showed similar isotope composition (close to zero or slightly negative odd-MIF; Feng et al., 2010, 2013) to the anthropogenic sources could also contribute to Hg_{PM}. Though it could not be excluded, the subtropical humid climate conditions especially the high relative humidity, frequent rainfall and high vegetation coverage would diminish the potential terrestrial (e.g. geogenic) particulate Hg input.

4.3.1. Event 1

The Hg_{PM} concentrations and its isotopic variation in event E1 showed the same similar tendency with those of the Hg_F (Fig. 1), which might be caused by the variation of similar sources as the filtered phases. Especially, the Hg derived from the western long-range transport with high odd-MIF contributed to the positive odd-MIF of event E1 Hg_{PM} as well. The lower MDF and odd-MIF in Hg_{PM} than in Hg_F likely indicated that the local anthropogenic Hg emission was the dominating contribution to particulate Hg content.

4.3.2. Event 2

The high Hg_{PM} concentration and its isotopic variation in event E2 showed the same similar tendency with that of the Hg_F (Fig. 1), which probably suggested the control by the same source input, in particular the incense combustion emission. Before the rain on this day, the air relative humidity was above 85%, which would lead to the incomplete combustion of the incense. Therefore, a high fraction of particulate Hg would be eventually emitted into the ABL and largely contribute to E2 Hg_{PM} through wet deposition scavenging (Obrist et al., 2008). Thus, both Hg_{PM} concentrations and its isotopic composition were largely impacted by the pollution of the occasional incense combustion event.

4.3.3. Event 3

In comparison with Hg_F, the Hg_{PM} concentrations and its proportion to total Hg were very low in E3 rain samples, due to the dilution of large precipitation amount and frequent wet scavenging in this wet season. Isotopically, both the MDF and odd-MIF of E3 Hg_{PM} increased with time (Fig. 1). Although the exact factors inducing the difference in Hg isotope variation between filtered and particulate phases remained unclear at this stage, the near zero odd-MIF of E3 Hg_{PM} at the starting and middle stages of this event suggested a relatively larger contribution of locally emitted anthropogenic particulate Hg. The relatively higher Δ^{199}Hg (0.28‰) found in sample E3-R4 collected at the end of E3 event was

likely to result from an increasing contribution of long-range transported Hg. This was further confirmed by the relatively higher Δ^{200}Hg (0.16‰, Table 1) in this sample (Cai and Chen, 2016; Chen et al., 2012).

To conclude, the Hg_{PM} should be investigated separately when studying mercury and its isotope systematics in precipitation, as it might occupy a large proportion of THg. Since Hg_{PM} has relatively lower Δ^{199}Hg, the filtered rain samples would display higher odd-MIF. Thus, despite the large difference in contributing sources, and in meteorological and geographical conditions, filtration could be another factor explaining the higher odd-MIF in the filtered rainwater (average $\Delta^{199}Hg = 0.54 \pm 0.59‰$, 2sd, $n = 24$) (Chen et al., 2012) than unfiltered rainwater (average $\Delta^{199}Hg = 0.28 \pm 0.49‰$, 2sd, $n = 114$) (Demers et al., 2013; Donovan et al., 2013; Gratz et al., 2010; Sherman et al., 2012, 2015) from North American. Rainwater samples should be filtered in future studies on precipitation Hg isotopes in order to obtain a better comparison and establish a more precise global biogeochemical model of Hg isotopes.

5. Conclusion

In this study, Hg isotopic compositions of the filtered Hg and, for the first time the particulate Hg of the same sequential rain sample were measured for three distinctive single rainfall events in Guiyang City, China. The total variation ranges of both MDF and odd-MIF were consistent with our previous study on the annual monitoring of Hg isotopes in Guiyang precipitation, suggesting continuous contribution from fixed Hg sources (both local and long-term transport). Interestingly, the rainwater Hg captured both MDF and odd-MIF signatures of the incense burning on the Tomb Sweeping Day, implying that occasional anthropogenic events also contribute to atmospheric Hg budget, and Hg isotopic compositions in precipitation are very sensitive to such momentous anthropogenic activities. Thus, occasional emission should be taken into account in future studies on the regional or global biogeochemical cycle of Hg. Our data, together with that reported in our previous study on Lhasa precipitation, showed that large variation of Hg isotopes might be a global phenomenon for sequential precipitation sampling, for both filtered and particulate phases, which should be both investigated and considered in future studies. Though further research is required for systematically studying the exchange dynamic of Hg and its isotopes between rainwater and particles in precipitation, our result showed that the large variations of Hg isotopes in both phases were more likely caused by change of source contribution, rather than atmospheric processes. The distinctive Hg isotopic composition (lower Δ^{199}Hg) of particulate phase compared to the filtered phase were inclined to be a large contribution to Hg_{PM} of sources with insignificant odd-MIF, likely the local anthropogenic emission. Our study demonstrated that instantaneous meteorological condition change would partially contribute to the large variation of Hg isotopic composition in precipitation, through for example changing the contributing proportion of variable sources, and that Hg isotopes, as stable H and O isotopes, could also provide a new horizon for local or regional meteorological research.

Acknowledgement

We thank Gyozo Jordan for English corrections and thorough reviews. The authors wish to acknowledge the associated editor Mae Sexauer Gustin and three anonymous reviewers who provided very useful comments and greatly improved the quality of the manuscript. This research was funded by Natural Science Foundation of China (41625012, 41273023, U1612442), and "Strategic Priority Research Program" (No. XDB05030302) project of Chinese Academy of Sciences.

Appendix A. Supplementary data

Supplementary data to this article can be found online at https://doi.org/10.1016/j.scitotenv.2017.12.082.

References

Bergquist, B.A., Blum, J.D., 2007. Mass-dependent and -independent fractionation of Hg isotopes by photoreduction in aquatic systems. Science 318 (5849):417–420. https://doi.org/10.1126/science.1148050.
Biswas, A., Blum, J.D., Bergquist, B.A., Keeler, G.J., Xie, Z., 2008. Natural mercury isotope variation in coal deposits and organic soils. Environ. Sci. Technol. 42 (22):8303–8309. https://doi.org/10.1021/es801444b.
Blum, J.D., Bergquist, B.A., 2007. Reporting of variations in the natural isotopic composition of mercury. Anal. Bioanal. Chem. 388 (2):353–359. https://doi.org/10.1007/s00216-007-1236-9.
Blum, J.D., Sherman, L.S., Johnson, M.W., 2014. Mercury isotopes in earth and environmental sciences. Annu. Rev. Earth Planet. Sci. 42 (1):249–269. https://doi.org/10.1146/annurev-earth-050212-124107.
Brunke, E.-G., Walters, C., Mkololo, T., Martin, L., Labuschagne, C., Silwana, B., Slemr, F., Weigelt, A., Ebinghaus, R., Somerset, V., 2016. Mercury in the atmosphere and in rainwater at Cape Point, South Africa. Atmos. Environ. 125:24–32. https://doi.org/10.1016/j.atmosenv.2015.10.059.
Cai, H., Chen, J., 2016. Mass-independent fractionation of even mercury isotopes. Sci. Bull. 61 (2):116–124. https://doi.org/10.1007/s11434-015-0968-8.
Celle-Jeanton, H., Gonfiantini, R., Travi, Y., Sol, B., 2004. Oxygen-18 variations of rainwater during precipitation: application of the Rayleigh model to selected rainfalls in Southern France. J. Hydrol. 289 (1–4):165–177. https://doi.org/10.1016/j.jhydrol.2003.11.017.
Chen, J., Hintelmann, H., Dimock, B., 2010. Chromatographic pre-concentration of Hg from dilute aqueous solutions for isotopic measurement by MC-ICP-MS. J. Anal. At. Spectrom. 25 (9):1402–1409. https://doi.org/10.1039/C0JA00014K.
Chen, J., Hintelmann, H., Feng, X., Dimock, B., 2012. Unusual fractionation of both odd and even mercury isotopes in precipitation from Peterborough, ON, Canada. Geochim. Cosmochim. Acta 90 (0):33–46. https://doi.org/10.1016/j.gca.2012.05.005.
Chen, J., Hintelmann, H., Zheng, W., Feng, X., Cai, H., Wang, Z., Yuan, S., Wang, Z., 2016. Isotopic evidence for distinct sources of mercury in lake waters and sediments. Chem. Geol. 426:33–44. https://doi.org/10.1016/j.chemgeo.2016.01.030.
Clarke, A.D., Freitag, S., Simpson, R.M.C., Hudson, J.G., Howell, S.G., Brekhovskikh, V.L., Campos, T., Kapustin, V.N., Zhou, J., 2013. Free troposphere as a major source of CCN for the equatorial pacific boundary layer: long-range transport and teleconnections. Atmos. Chem. Phys. 13 (15):7511–7529. https://doi.org/10.5194/acp-13-7511-2013.
Coplen, T.B., Neiman, P.J., White, A.B., Landwehr, J.M., Ralph, F.M., Dettinger, M.D., 2008. Extreme changes in stable hydrogen isotopes and precipitation characteristics in a landfalling Pacific storm. Geophys. Res. Lett. 35 (21):1–5. https://doi.org/10.1029/2008GL035481.
Craig, H., 1961. Isotopic variations in meteoric waters. Science 133 (3465):1702–1703. https://doi.org/10.1126/science.133.3465.1702.
Dansgaard, W., 1964. Stable isotopes in precipitation. Tellus 16 (4):436–468. https://doi.org/10.3402/tellusa.v16i4.8993.
Das, R., Landing, W., Bizimis, M., Odom, L., Caffrey, J., 2015. Mass independent fractionation of mercury isotopes as source tracers in sediments. Proc. Earth Planet. Sci. 13:151–157. https://doi.org/10.1016/j.proeps.2015.07.036.
Demers, J.D., Blum, J.D., Zak, D.R., 2013. Mercury isotopes in a forested ecosystem: implications for air-surface exchange dynamics and the global mercury cycle. Glob. Biogeochem. Cycles 27 (1):222–238. https://doi.org/10.1002/gbc.20021.
Demers, J.D., Sherman, L.S., Blum, J.D., Marsik, F.J., Dvonch, J.T., 2015. Coupling atmospheric mercury isotope ratios and meteorology to identify sources of mercury impacting a coastal urban-industrial region near Pensacola, Florida, USA. Glob. Biogeochem. Cycles 29 (10):1689–1705. https://doi.org/10.1002/2015GB005146.
Donovan, P.M., Blum, J.D., Yee, D., Gehrke, G.E., Singer, M.B., 2013. An isotopic record of mercury in San Francisco Bay sediment. Chem. Geol. 349:87–98. https://doi.org/10.1016/j.chemgeo.2013.04.017.
Enrico, M., Le Roux, G., Marusczak, N., Heimburger, L.-E., Claustres, A., Fu, X., Sun, R., Sonke, J.E., 2016. Atmospheric mercury transfer to peat bogs dominated by gaseous elemental mercury dry deposition. Environ. Sci. Technol. 50 (5):2405–2412. https://doi.org/10.1021/acs.est.5b06058.
Enrico, M., Le Roux, G., Heimburger, L.-E., Van Beek, P., Souhaut, M., Chmeleff, J., Sonke, J.E., 2017. Holocene atmospheric mercury levels reconstructed from peat bog mercury stable isotopes. Environ. Sci. Technol. 51 (11):5899–5906. https://doi.org/10.1021/acs.est.6b05804.
EPA, U., 2002. Method 1631, Revision E: Mercury in Water by Oxidation, Purge and Trap, and Cold Vapor Atomic Fluorescence Spectrometry. US Environmental Protection Agency Washington, DC.
Fang, G.-C., Chang, C.-N., Wu, Y.-S., Yang, C.-J., Chang, S.-C., Yang, I.L., 2002. Suspended particulate variations and mass size distributions of incense burning at Tzu Yun Yen temple in Taiwan, Taichung. Sci. Total Environ. 299 (1–3):79–87. https://doi.org/10.1016/S0048-9697(02)00227-9.
Felix, J.D., Elliott, E.M., Avery, G.B., Kieber, R.J., Mead, R.N., Willey, J.D., Mullaugh, K.M., 2015. Isotopic composition of nitrate in sequential hurricane Irene precipitation samples: implications for changing NOx sources. Atmos. Environ. 106 (0):191–195. https://doi.org/10.1016/j.atmosenv.2015.01.075.
Feng, X., Foucher, D., Hintelmann, H., Yan, H., He, T., Qiu, G., 2010. Tracing mercury contamination sources in sediments using mercury isotope compositions. Environ. Sci. Technol. 44 (9):3363–3368. https://doi.org/10.1021/es9039488.
Feng, X., Bai, W., Shang, L., He, T., Qiu, G., Yan, H., 2011. Mercury speciation and distribution in Aha Reservoir which was contaminated by coal mining activities in Guiyang, Guizhou, China. Appl. Geochem. 26 (2):213–221. https://doi.org/10.1016/j.apgeochem.2010.11.021.
Feng, X., Yin, R., Yu, B., Du, B., 2013. Mercury isotope variations in surface soils in different contaminated areas in Guizhou Province, China. Chin. Sci. Bull. 58 (2):249–255. https://doi.org/10.1007/s11434-012-5488-1.

Fu, X., Feng, X., Qiu, G., Shang, L., Zhang, H., 2011. Speciated atmospheric mercury and its potential source in Guiyang, China. Atmos. Environ. 45 (25):4205–4212. https://doi.org/10.1016/j.atmosenv.2011.05.012.
Giang, A., Selin, N.E., 2015. Benefits of mercury controls for the United States. Proc. Natl. Acad. Sci. 201514395. https://doi.org/10.1073/pnas.1514395113.
Gratz, L.E., Keeler, G.J., Miller, E.K., 2009. Long-term relationships between mercury wet deposition and meteorology. Atmos. Environ. 43 (39):6218–6229. https://doi.org/10.1016/j.atmosenv.2009.08.040.
Gratz, L.E., Keeler, G.J., Blum, J.D., Sherman, L.S., 2010. Isotopic composition and fractionation of mercury in great lakes precipitation and ambient air. Environ. Sci. Technol. 44 (20):7764–7770. https://doi.org/10.1021/es100383w.
Gratz, L.E., Ambrose, J.L., Jaffe, D.A., Shah, V., Jaeglé, L., Stutz, J., Festa, J., Spolaor, M., Tsai, C., Selin, N.E., Song, S., Zhou, X., Weinheimer, A.J., Knapp, D.J., Montzka, D.D., Flocke, F.M., Campos, T.L., Apel, E., Hornbrook, R., Blake, N.J., Hall, S., Tyndall, G.S., Reeves, M., Stechman, D., Stell, M., 2015. Oxidation of mercury by bromine in the subtropical Pacific free troposphere. Geophys. Res. Lett. 42 (23):10,494–10,502. https://doi.org/10.1002/2015GL066645.
Gray, J.E., Pribil, M.J., Van Metre, P.C., Borrok, D.M., Thapalia, A., 2013. Identification of contamination in a lake sediment core using Hg and Pb isotopic compositions, Lake Ballinger, Washington, USA. Appl. Geochem. 29:1–12. https://doi.org/10.1016/j.apgeochem.2012.12.001.
Gray, J.E., Van Metre, P.C., Pribil, M.J., Horowitz, A.J., 2015. Tracing historical trends of Hg in the Mississippi River using Hg concentrations and Hg isotopic compositions in a lake sediment core, Lake Whittington, Mississippi, USA. Chem. Geol. 395:80–87. https://doi.org/10.1016/j.chemgeo.2014.12.005.
Huang, J., Kang, S., Zhang, Q., Yan, H., Guo, J., Jenkins, M.G., Zhang, G., Wang, K., 2012. Wet deposition of mercury at a remote site in the Tibetan Plateau: concentrations, speciation, and fluxes. Atmos. Environ. 62 (0):540–550. https://doi.org/10.1016/j.atmosenv.2012.09.003.
Huang, J., Kang, S., Wang, S., Wang, L., Zhang, Q., Guo, J., Wang, K., Zhang, G., Tripathee, L., 2013. Wet deposition of mercury at Lhasa, the capital city of Tibet. Sci. Total Environ. 447 (0):123–132. https://doi.org/10.1016/j.scitotenv.2013.01.003.
Huang, Q., Liu, Y., Chen, J., Feng, X., Huang, W., Yuan, S., Cai, H., Fu, X., 2015. An improved dual-stage protocol to pre-concentrate mercury from airborne particles for precise isotopic measurement. J. Anal. At. Spectrom. 30 (4):957–966. https://doi.org/10.1039/c4ja00438h.
Jaffe, D., Prestbo, E., Swartzendruber, P., Weiss-Penzias, P., Kato, S., Takami, A., Hatakeyama, S., Kajii, Y., 2005. Export of atmospheric mercury from Asia. Atmos. Environ. 39 (17) http://doi.org/3029-3038. https://doi.org/10.1016/j.atmosenv.2005.01.030.
Jetter, J.J., Guo, Z., McBrian, J.A., Flynn, M.R., 2002. Characterization of emissions from burning incense. Sci. Total Environ. 295 (1–3):51–67. https://doi.org/10.1016/S0048-9697(02)00043-8.
Keil, A., Berking, J., Mügler, I., Schütt, B., Schwalb, A., Steeb, P., 2010. Hydrological and geomorphological basin and catchment characteristics of Lake Nam Co, South-Central Tibet. Quat. Int. 218 (1–2):118–130. https://doi.org/10.1016/j.quaint.2009.02.022.
Koster van Groos, P.G., Esser, B.K., Williams, R.W., Hunt, J.R., 2013. Isotope effect of mercury diffusion in air. Environ. Sci. Technol. 48 (1):227–233. https://doi.org/10.1021/es4033666.
Landing, W.M., Caffrey, J.M., Nolek, S.D., Gosnell, K.J., Parker, W.C., 2010. Atmospheric wet deposition of mercury and other trace elements in Pensacola, Florida. Atmos. Chem. Phys. 10 (10):4867–4877. https://doi.org/10.5194/acp-10-4867-2010.
Landis, M.S., Ryan, J.V., ter Schure, A.F.H., Laudal, D., 2014. Behavior of mercury emissions from a commercial coal-fired power plant: the relationship between stack speciation and near-field plume measurements. Environ. Sci. Technol. 48 (22):13540–13548. https://doi.org/10.1021/es500783t.
Li, J., Tao, T., Pang, Z., Tan, M., Kong, Y., Duan, W., Zhang, Y., 2015. Identification of different moisture sources through isotopic monitoring during a storm event. J. Hydrometeorol. 16 (4):1918–1927. https://doi.org/10.1175/JHM-D-15-0005.1.
Lin, H., Yuan, D., Lu, B., Huang, S., Sun, L., Zhang, F., Gao, Y., 2015. Isotopic composition analysis of dissolved mercury in seawater with purge and trap preconcentration and a modified Hg introduction device for MC-ICP-MS. J. Anal. At. Spectrom. 30 (2): 353–359. https://doi.org/10.1039/c4ja00242c.
Liu, J., Feng, X., Yin, R., Zhu, W., Li, Z., 2011. Mercury distributions and mercury isotope signatures in sediments of Dongjiang, the Pearl River Delta, China. Chem. Geol. 287 (1–2): 81–89. https://doi.org/10.1016/j.chemgeo.2011.06.001.
Liu, N., Qiu, G., Landis, M.S., Feng, X., Fu, X., Shang, L., 2011. Atmospheric mercury species measured in Guiyang, Guizhou province, southwest China. Atmos. Res. 100 (1): 93–102. https://doi.org/10.1016/j.atmosres.2011.01.002.
Lynam, M.M., Dvonch, J.T., Hall, N.L., Morishita, M., Barres, J.A., 2014. Spatial patterns in wet and dry deposition of atmospheric mercury and trace elements in central Illinois, USA. Environ. Sci. Pollut. Res. 21 (6):4032–4043. https://doi.org/10.1007/s11356-013-2011-4.
Marumoto, K., Matsuyama, A., 2014. Mercury speciation in wet deposition samples collected from a coastal area of Minamata Bay. Atmos. Environ. 86:220–227. https://doi.org/10.1016/j.atmosenv.2013.12.011.
Munksgaard, N.C., Wurster, C.M., Bass, A., Bird, M.I., 2012. Extreme short-term stable isotope variability revealed by continuous rainwater analysis. Hydrol. Process. 26 (23): 3630–3634. https://doi.org/10.1002/hyp.9505.
Nair, U.S., Wu, Y., Holmes, C.D., Ter Schure, A., Kallos, G., Walters, J.T., 2013. Cloud-resolving simulations of mercury scavenging and deposition in thunderstorms. Atmos. Chem. Phys. 13 (19):10143–10157. https://doi.org/10.5194/acp-13-10143-2013.
Nzihou, A., Stanmore, B., 2013. The fate of heavy metals during combustion and gasification of contaminated biomass—a brief review. J. Hazard. Mater. 256–257:56–66. https://doi.org/10.1016/j.jhazmat.2013.02.050.
Obrist, D., Moosmüller, H., Schürmann, R., Chen, L.W.A., Kreidenweis, S.M., 2008. Particulate-phase and gaseous elemental mercury emissions during biomass combustion: controlling factors and correlation with particulate matter emissions. Environ. Sci. Technol. 42 (3):721–727. https://doi.org/10.1021/es071279n.
Obrist, D., Agnan, Y., Jiskra, M., Olson, C.L., Colegrove, D.P., Hueber, J., Moore, C.W., Sonke, J.E., Helmig, D., 2017. Tundra uptake of atmospheric elemental mercury drives Arctic mercury pollution. Nature 547 (7662):201–204. https://doi.org/10.1038/nature22997.
Poissant, L., Pilote, M., 1998. Mercury concentrations in single event precipitation in southern Québec. Sci. Total Environ. 213 (1–3):65–72. https://doi.org/10.1016/S0048-9697(98)00076-X.
Rolison, J.M., Landing, W.M., Luke, W., Cohen, M., Salters, V.J.M., 2013. Isotopic composition of species-specific atmospheric Hg in a coastal environment. Chem. Geol. 336 (0): 37–49. https://doi.org/10.1016/j.chemgeo.2012.10.007.
Sanei, H., Outridge, P.M., Goodarzi, F., Wang, F., Armstrong, D., Warren, K., Fishback, L., 2010. Wet deposition mercury fluxes in the Canadian sub-Arctic and southern Alberta, measured using an automated precipitation collector adapted to cold regions. Atmos. Environ. 44 (13):1672–1681. https://doi.org/10.1016/j.atmosenv.2010.01.030.
Schroeder, W.H., Munthe, J., 1998. Atmospheric mercury—an overview. Atmos. Environ. 32 (5):809–822. https://doi.org/10.1016/S1352-2310(97)00293-8.
Seo, Y.S., Han, Y.J., Choi, H.D., Holsen, T.M., Yi, S.M., 2012. Characteristics of total mercury (TM) wet deposition: scavenging of atmospheric mercury species. Atmos. Environ. 49:69–76. https://doi.org/10.1016/j.atmosenv.2011.12.031.
Shen, H., Tsai, C.-M., Yuan, C.-S., Jen, Y.-H., Ie, I.-R., 2017. How incense and joss paper burning during the worship activities influences ambient mercury concentrations in indoor and outdoor environments of an Asian temple? Chemosphere 167:530–540. https://doi.org/10.1016/j.chemosphere.2016.09.159.
Sherman, L.S., Blum, J.D., Keeler, G.J., Demers, J.D., Dvonch, J.T., 2012. Investigation of local mercury deposition from a coal-fired power plant using mercury isotopes. Environ. Sci. Technol. 46 (1):382–390. https://doi.org/10.1021/es202793c.
Sherman, L.S., Blum, J.D., Dvonch, J.T., Gratz, L.E., Landis, M.S., 2015. The use of Pb, Sr, and Hg isotopes in Great Lakes precipitation as a tool for pollution source attribution. Sci. Total Environ. 502 (0):362–374. https://doi.org/10.1016/j.scitotenv.2014.09.034.
Sun, R., Sonke, J.E., Heimbürger, L.-E., Belkin, H.E., Liu, G., Shome, D., Cukrowska, E., Liousse, C., Pokrovsky, O.S., Streets, D.G., 2014. Mercury stable isotope signatures of world coal deposits and historical coal combustion emissions. Environ. Sci. Technol. 48 (13): 7660–7668. https://doi.org/10.1021/es501208a.
Sun, R., Streets, D.G., Horowitz, H.M., Amos, H.M., Liu, G., Perrot, V., Toutain, J.-P., Hintelmann, H., Sunderland, E.M., Sonke, J.E., 2016. Historical (1850–2010) mercury stable isotope inventory from anthropogenic sources to the atmosphere. Elem. Sci. Anthropocene 4 (1), 000091. https://doi.org/10.12952/journal.elementa.000091.
Tong, Y., Eichhorst, T., Olson, M.R., Rutter, A.P., Shafer, M.M., Wang, X., Schauer, J.J., 2014. Comparison of heterogeneous photolytic reduction of Hg(II) in the coal fly ashes and synthetic aerosols. Atmos. Res. 138:324–329. https://doi.org/10.1016/10.1016/j.atmosres.2013.11.015.
Tsui, M.T.K., Blum, J.D., Kwon, S.Y., Finlay, J.C., Balogh, S.J., Nollet, Y.H., 2012. Sources and transfers of methylmercury in adjacent river and forest food webs. Environ. Sci. Technol. 46 (20):10957–10964. https://doi.org/10.1021/es3019836.
Walters, D.M., Raikow, D.F., Hammerschmidt, C.R., Mehling, M.G., Kovach, A., Oris, J.T., 2015. Methylmercury bioaccumulation in stream food webs declines with increasing primary production. Environ. Sci. Technol. 49 (13):7762–7769. https://doi.org/10.1021/acs.est.5b00911.
Wang, B., Lee, S.C., Ho, K.F., Kang, Y.M., 2007. Characteristics of emissions of air pollutants from burning of incense in temples, Hong Kong. Sci. Total Environ. 377 (1):52–60. https://doi.org/10.1016/j.scitotenv.2007.01.099.
Wang, F., Wang, S., Zhang, L., Yang, H., Wu, Q., Hao, J., 2014. Mercury enrichment and its effects on atmospheric emissions in cement plants of China. Atmos. Environ. 92 (0): 421–428. https://doi.org/10.1016/j.atmosenv.2014.04.029.
Wang, X., Zhang, H., Lin, C.-J., Fu, X., Zhang, Y., Feng, X., 2015. Transboundary transport and deposition of Hg emission from springtime biomass burning in the Indo-China Peninsula. J. Geophys. Res. Atmos. 120 (18):9758–9771. https://doi.org/10.1002/2015JD023525.
Wang, Z., Chen, J., Feng, X., Hintelmann, H., Yuan, S., Cai, H., Huang, Q., Wang, S., Wang, F., 2015. Mass-dependent and mass-independent fractionation of mercury isotopes in precipitation from Guiyang, SW China. Compt. Rendus Geosci. 347 (7–8):358–367. https://doi.org/10.1016/j.crte.2015.02.006.
Weiss-Penzias, P., Gustin, M.S., Lyman, S.N., 2009. Observations of speciated atmospheric mercury at three sites in Nevada: evidence for a free tropospheric source of reactive gaseous mercury. J. Geophys. Res. Atmos. 114 (D14), D14302. https://doi.org/10.1029/2008JD011607.
White, E.M., Keeler, G.J., Landis, M.S., 2009. Spatial variability of mercury wet deposition in Eastern Ohio: summertime meteorological case study analysis of local source influences. Environ. Sci. Technol. 43 (13):4946–4953. https://doi.org/10.1021/es803214h.
White, E.M., Landis, M.S., Keeler, G.J., Barres, J.A., 2013. Investigation of mercury wet deposition physicochemistry in the Ohio River Valley through automated sequential sampling. Sci. Total Environ. 448:107–119. https://doi.org/10.1016/j.scitotenv.2012.12.046.
Wiederhold, J.G., Cramer, C.J., Daniel, K., Infante, I., Bourdon, B., Kretzschmar, R., 2010. Equilibrium mercury isotope fractionation between dissolved Hg(II) species and thiol-bound Hg. Environ. Sci. Technol. 44 (11):4191–4197. https://doi.org/10.1021/es100205t.
Yin, R., Feng, X., Meng, B., 2013. Stable mercury isotope variation in rice plants (*Oryza sativa* L.) from the Wanshan Mercury Mining District, SW China. Environ. Sci. Technol. 47 (5):2238–2245. https://doi.org/10.1021/es304302a.
Yin, R., Feng, X., Chen, J., 2014. Mercury stable isotopic compositions in coals from major coal producing fields in china and their geochemical and environmental implications. Environ. Sci. Technol. 48 (10):5565–5574. https://doi.org/10.1021/es500322n.
Yu, B., Fu, X., Yin, R., Zhang, H., Wang, X., Lin, C.-J., Wu, C., Zhang, Y., He, N., Fu, P., Wang, Z., Shang, L., Sommar, J., Sonke, J.E., Maurice, L., Guinot, B., Feng, X., 2016. Isotopic composition of atmospheric mercury in China: new evidence for source and transformation

processes in air and in vegetation. Environ. Sci. Technol. 50 (17):9262–9269. https://doi.org/10.1021/acs.est.6b01782.

Yuan, S., Zhang, Y., Chen, J., Kang, S., Zhang, J., Feng, X., Cai, H., Wang, Z., Wang, Z., Huang, Q., 2015. Large variation of mercury isotope composition during a single precipitation event at Lhasa City, Tibetan Plateau, China. Proc. Earth Planet. Sci. 13:282–286. https://doi.org/10.1016/j.proeps.2015.07.066.

Zhang, G., Zhou, L., Zheng, X., Huang, W., Wang, Y., Qian, P., 2010. Spatio-temporal distribution law of mercury in wet deposition and its influencing factors in summer of Shanghai. Environ. Sci. Technol. 33 (7):7–11,60. https://doi.org/10.3969/j.issn.1003-6504.2010.07.002.

Zhang, H., Fu, X.W., Lin, C.J., Wang, X., Feng, X.B., 2015. Observation and analysis of speciated atmospheric mercury in Shangri-La, Tibetan Plateau, China. Atmos. Chem. Phys. 15 (2):653–665. https://doi.org/10.5194/acp-15-653-2015.

Zheng, W., Hintelmann, H., 2009. Mercury isotope fractionation during photoreduction in natural water is controlled by its Hg/DOC ratio. Geochim. Cosmochim. Acta 73 (22): 6704–6715. https://doi.org/10.1016/j.gca.2009.08.016.

Zheng, W., Hintelmann, H., 2010. Isotope fractionation of mercury during its photochemical reduction by low-molecular-weight organic compounds. J. Phys. Chem. A 114 (12): 4246–4253. https://doi.org/10.1021/jp9111348.

Zhou, J., Feng, X., Liu, H., Zhang, H., Fu, X., Bao, Z., Wang, X., Zhang, Y., 2013. Examination of total mercury inputs by precipitation and litterfall in a remote upland forest of Southwestern China. Atmos. Environ. 81:364–372. https://doi.org/10.1016/j.atmosenv.2013.09.010.